Design and manufacturing of high-strain P(VDF-TrFE-CTFE) actuators

Gallucci, Giulio; Jaarsma, Victor; Hunt, Andres

DOI
10.1117/12.3010459

Publication date
2024

Document Version
Final published version

Published in
Electroactive Polymer Actuators and Devices (EAPAD) XXVI

Design and manufacturing of high-strain P(VDF-TrFE-CTFE) actuators

Giulio Gallucci, Victor Jaarsma, and Andres Hunt

Department of Precision and Microsystems Engineering, Delft University of Technology, Mekelweg 2, 2628CD Delft, The Netherlands

ABSTRACT

High strains of the relaxor ferroelectric polymers allows to build efficient actuators. While the mechanical impedance of such actuators can be optimized via their morphology, their practical realization requires flexible and versatile fabrication processes. This work devises an efficient procedure for manufacturing unimorph bending actuators basing on the P(VDF-TrFE-CTFE) electroactive polymer (EAP). The fabrication process consists of inkjet printing the Ag electrodes and stencil printing the active P(VDF-TrFE-CTFE) layer. The effect of constituent layer dimensions and properties are analytically modelled to estimate the optimal morphology for highest strains. Actuators are manufactured on polyethylene naphthalate (PEN) and polyethylene terephthalate (PET) substrates and their performance is characterized. On PET substrate, the EAP layer thicknesses of 5 μm up to 24 μm are studied. The PEN-based actuators achieved up to 759 μm deflections in quasi-static (1 Hz, 560 V_{pp}) and up to 5.95 mm in resonant operation (52 Hz, 550 V_{pp}). The PET-based actuators achieved up to 486 μm deflections in quasi-static (1 Hz, 980 V_{pp}) and up to 4.44 mm in resonant operation (116 Hz, 700 V_{pp}). These results indicate an up to 123% improvement in quasi-static and 60% resonant actuation strains compared to the previously reported similar actuators. Modelling predicts that significantly larger deflections are feasible when fabricating the transducers with optimized morphology.

Keywords: Electroactive polymer, actuator, fabrication, P(VDF-TrFE-CTFE), relaxor ferroelectric, inkjet printing, stencil printing, structure

1. INTRODUCTION

Smart material sensors and actuators provide a versatile complement to the conventional transducers, enabling innovation in robotics,[1] life sciences[2–4] and many more fields.[5–7] Electroactive polymers (EAPs, a class of polymeric smart materials) are capable of converting electrical energy into mechanical deformation and/or vice versa.[8] They are simple in construction, low in stiffness, exhibit large deformations (significantly above the conventional piezoceramics), and can be directly coupled to electronic circuits.[9,10]

P(VDF-TrFE-CTFE) is a relaxor ferroelectric polymer of electronic EAP type that exhibits up to 5% material strains.[11] They belong in the group of electronic EAPs, typically characterized by high bandwidth and energy efficiency, but often limited in the range of deformation.[12,13] In contrast, the ionic EAPs operate at much lower excitation voltages, exhibit larger material strains, but are limited in bandwidth and energy efficiency.[14] Constructing versatile transducers from P(VDF-TrFE-CTFE) materials (and smart materials in general) requires efficient designs that couple the material strain to the transducer input or output[15,16] and efficient methods to fabricate them.

Different manufacturing methods have been employed for fabricating PVDF-based actuators, such as doctor-blading,[17] spin coating,[18] solution casting,[19] dip coating,[20] inkjet printing[21] and airbrush printing.[22] Each method offers a specific trade-off between the equipment cost, labour-intensity, design flexibility, attainable

Further author information: (Send correspondence to A.H.)
G.G.: E-mail: g.gallucci@tudelft.nl
V.J.: E-mail: victorjaarsma@hotmail.com
A.H.: E-mail: a.hunt@tudelft.nl

Electroactive Polymer Actuators and Devices (EAPAD) XXVI, edited by John D. W. Madden, Proc. of SPIE Vol. 12945, 1294503
 · 0277-786X · doi: 10.1117/12.3010459

geometries, resolution, wastage and other factors. The choice of best-suited process depends on the objective and available resources, and is often a combination of different methods.

Stencil printing is a simple and versatile technique for printing thin films, commonly used to apply solder paste on printed circuit boards.[23] It has been proposed for depositing polymer solutions in metamaterial fabrication,[24] and could also be used for EAP deposition. While it is a contact-based fabrication method that requires design-specific stencils and offers much less flexibility than additive manufacturing methods, its benefits include (1) higher design flexibility than in doctorblading, spin coating or dip coating, (2) better attainable layer quality than in screen printing, and (3) better affordability of the required equipment than in additive manufacturing methods.

This study proposes an efficient process for fabricating P(VDF-TrFE-CTFE) actuators, and employs it to manufactures such relaxor ferroelecric actuators capable of large bending strains. The actuators are designed basing on the unimorph bending cantilever concept, considering the impact of morphology on actuation displacements (Section 2.1). Actuator fabrication employs PEN and PET-based substrates, Ag nanoparticle inks for electrodes, and P(VDF-TrFE-CTFE) for EAP (Section 2.2). The fabrication process combines inkjet printing for electrode deposition, stencil printing for EAP deposition, and additional processing steps to ensure curing and adhesion of the materials (Section 2.3). Cantilever actuators are produced at 5 μm to 24 μm EAP layer thicknesses on the PET-based substrate, and at 10 μm EAP thickness on PEN substrate, controlled by the stencil thickness. Morphology of the resulting actuators is studied by exposing their cross-section and imaging in SEM (Section 2.4). Actuation performance is characterized by measuring the frequency response, quasi-static voltage-deflection characteristics and breakdown strength (Section 2.4). The results are presented in Section 3, discussed in Section 4, and the paper is concluded in Section 5.

2. MATERIALS AND METHODS

2.1 Actuator design

This study bases on the bending unimorph actuator morphology, essentially consisting of a passive substrate and an active functional layer. In practice, a total of four layers is required, i.e. the passive substrate, the bottom electrode, the active EAP layer and the top electrode, whereas the two electrodes are needed to apply electric field on the EAP layer. The actuator design and dimensions are shown in Figure 1, indicating the 18 mm by 3 mm cantilever actuator portion, and the wider base that is used for mechanical clamping and electrical connections. Upon application of the electric field, the EAP layer is compressed in thickness, elongates in length, and causes the actuator tip to bend in the substrate direction.

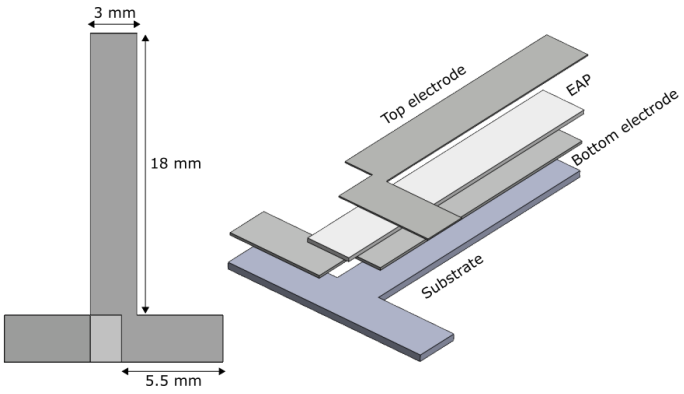

Figure 1. Design and dimensions of the unimorph bending actuator.

Attainable tip deflections of a unimorph cantilever actuator depend on several factors. Besides the attainable EAP material strains, the Young's moduli and thicknesses of the actuator components need to be accounted.

Maximum deflection δ can be analytically expressed as:[16,25]

$$\delta = \frac{3L^2}{2t} \cdot \frac{2AB(1+B)^2}{A^2B^4 + 2AB(2+3B+2B^2)+1} \cdot S_1, \quad A = \frac{Y_{sub}}{Y_{act}}, \quad B = \frac{t_{sub}}{t_{act}}, \tag{1}$$

where L and t are the length and thickness of the unimorph, S_1 is the transverse strain of the active film; Y_{sub} and Y_{act} are the Young's moduli of the substrate and the active layer; and t_{sub} and t_{act} the thicknesses of the respective layers. This model is valid for small tip displacements and accounts only for the substrate and active layers. The effect of the electrodes can omitted since they are very thin and do not attain the full stiffness of the bulk Ag metal.

This model is employed to predict the performance of the fabricated actuators and the outlooks for improving their performance. Modelling bases on the polyethylene naphthalate (PEN) and polyethylene terephthalate (PET) substrates that are used in actuator fabrication (respectively 50 μm and 140 μm in thickness, see Section 2.2), and estimates the actuator tip displacement as a function of the EAP layer thickness. Young's modulus of PEN and PET varies, depending on the exact polymer composition, and is assumed to be 3 GPa for both substrates. For the EAP layer, a transverse strain of 0.5% is used (this is well below the 5% max strain of the EAP[11]) and the Young's modulus is assumed to be 0.150 GPa (as reported by Schiava *et al.*[25]).

2.2 Materials

Actuator fabrication bases on two substrates. The first one is Novele IJ-220 (Novacentrix), a PET sheet with a microporous resin coating and a total thickness of 140 ± 12 μm,[26] specifically designed for inkjet printing of conductive inks. The second substrate is a 50 μm thick PEN (Goodfellow). Unlike the IJ-220, PEN is hydrophobic and requires surface treatment in order to make the inks to stick and adhere on it.

The bottom electrodes are fabricated using Ag nanoparticle inks, with different inks employed on the two substrates. On PET (Novele IJ-220) the NBSIJ-MU01 (Mitsubishi Paper Mills Inc) ink with a 15% Ag loading factor is used.[27] This ink self-sinters when printed on the porous IJ-220 substrate, but cannot be printed on non-porous surfaces due to its low Ag content. On PEN substrate the Metalon JS-A211 ink (Novacentrix) with a 40% Ag content is employed to print the bottom electrode.[28] Although it requires thermal sintering at temperatures above $100°C$, it remains below the melting temperature of the EAP. The same ink (JS-A211) is later used to print the top electrode on the EAP layer.

The EAP layer fabrication bases on the P(VDF-TrFE-CTFE) polymer Piezotech RT-TS (62:31:7 mol%, Arkema).[11] To create a printable ink, the polymer powder is dissolved in methyl ethyl ketone (MEK, from Merck). The polymer powder is placed in a sealed container, and MEK is added at a mass ratio of 1:10. The powder dissolves completely within 24 hours without requiring any agitation. According to the manufacturer, P(VDF-TrFE-CTFE) has a melting temperature of $122°C$, and a Young's modulus ranging from 0.1 to 0.5 GPa. It is recommended to be annealed at $110°C$ for 5 min up to 2h.[11]

2.3 Fabrication

Actuator fabrication combines inkjet printing and stencil printing, respectively for depositing the conductive Ag nanoparticle inks and the relaxor ferroelectric EAP (Section 2.2). Manufacturing process consists of the following steps: (1) first, the bottom electrode is inkjet printed on the substrate (Section 2.3.1), (2) next, the P(VDF-TrFE-CTFE) is applied using stencil printing (Section 2.3.2), and (3) finally, the top electrode is inkjet printed onto the EAP layer (Section 2.3.3). The process is illustrated in Figure 2.

2.3.1 Bottom electrode

The fabrication process of the bottom electrode depends on the substrate material. On IJ-220, the electrode is printed from Mitsubishi NBSIJ-MU01 ink using a Dimatix DMC 11610 printhead. The ink self-sinters on the porous substrate and becomes conductive without requiring additional processing steps. However, the PEN substrate is hydrophobic and requires surface modification before an electrode can be printed on it. Laser-texturing polymer surfaces can be used to alter their surface energy,[29] and in this study a pattern of approximately 10 μm diameter dots with a 50 μm spacing is etched into the substrate using a femtosecond laser micromachining

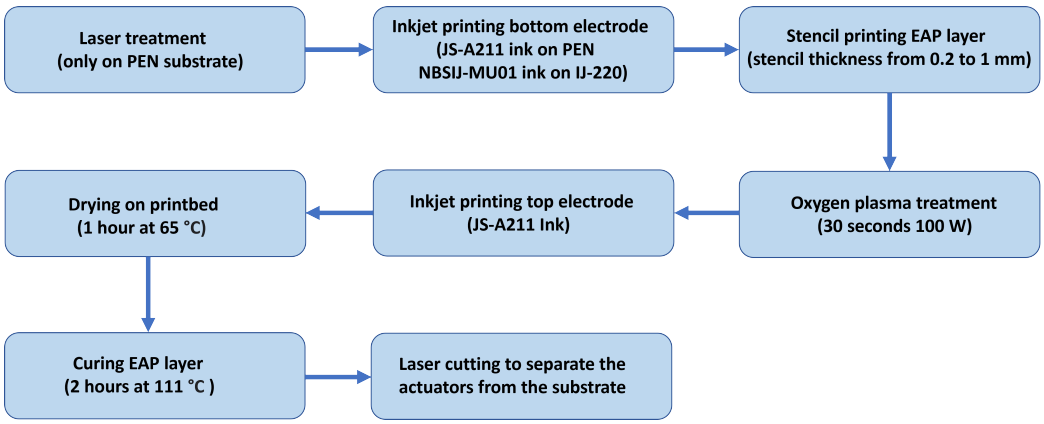

Figure 2. Actuator fabrication process.

system (Lasea LS Lab). This facilitates a good adhesion of the droplets on the surface. The bottom electrode is then printed using Metalon JS-A211 ink with a Dimatix Samba printhead, and thermally cured (identical to the top electrode curing in Section 2.3.3). Inkjet printing is performed on a Pixdro LP-50 platform, and the respective printing parameters are summarized in Table 1.

2.3.2 EAP layer

The EAP layer is fabricated by stencil printing, a process commonly employed in electronics for applying solder paste on PCBs.[23] It is a contact-based method that suits well for applying pastes and thick liquids. The stencil serves to mask the areas that should not be covered by ink, and ensures a precise offset between the substrate and the blade. The thickness of the resulting EAP layer is determined by the stencil thickness, printing repetitions and concentration of EAP in the ink. Steel stencils of different thicknesses (0.1 mm, 0.2 mm, 0.3 mm, 0.4 mm and 0.5 mm) are produced using a laser cutter (Lasea LS Lab), and two stencils are stacked to reach the stencil thicknesses of up to 1 mm (in 0.1 mm increments).

To print the EAP layer, a stencil is placed in contact with the substrate, aligned with the bottom electrode, and fixed in place by a magnetic block under the sample. EAP ink is loaded into a syringe, applied onto the stencil, and wiped using a microscopy slide. This squeezes the polymer into the stencil cavity, and removes the excess material. After 5 to 15 minutes (depending on the stencil thickness), the solvent partially dries, and the stencil can be lifted from the substrate. Samples are then placed in a desiccator overnight to evaporate the remaining solvent. The equipment for stencil printing the EAP layer is shown in Figure 3.

Table 1. Printing recipes for the conductive Ag nanoparticle inks.

	Ink	
Parameter	**NBSIJ-MU01**	**JS-A211**
Printhead	DMC 11610	Dimatix Samba
Substrates	Novele IJ-220	PEN and EAP
Print speed	60 mm/s	60 mm/s
Resolution	1000 DPI	1500 DPI
Native droplet volume	10 pL	2.4 pL
Measured droplet volume	14 pL	4 pL
Nozzles used during printing	1	12
Print repetitions	1	4
Print time	315 s	120 s

Figure 3. The stencil printing set-up. After completing the bottom electrode, the sample is placed between a magnetic block and a stencil (right). The polymer ink (glass bottle on the left) is loaded into a syringe (center), applied on the stencil, and wiped with a microscopy slide (bottom left).

2.3.3 Top electrode

To promote adhesion and prevent agglomeration of the ink during the printing of the top electrode, the hydrophobic surface of the EAP needs to be first turned hydrophilic. This is achieved by oxygen plasma treatment at 100 W power and 30 s exposure time (Diener Femto). The top electrode is then printed with Metalon JS-A211 ink using a Dimatix Samba printhead, according to the recipe summarized in Table 1. Next, the sample is placed in an oven and kept at $111°C$ for 2 hours (Memmert UN30), fusing the ink into a conductive sheet and annealing the EAP layer ($111°C$ is the middle temperature between the lowest recommended sintering temperature for the Ag ink[28] and the melting temperature of the EAP[11]). The finished actuator is separated from the substrate by laser ablation (Lasea LS Lab).

2.4 Characterization

Characterization of the resulting actuator samples studies their structure and actuation capabilities. To study the actuator structure, its cross-section is first exposed using a femtosecond laser micromachining tool (Lasea LS Lab). Laser ablation is implemented at low average powers to promote material removal and prevent melting of the adjacent structures in the sample. The cross-section is visualized in SEM (Jeol JSM 6010LA) to study the actuators and measure the thicknesses of the constituent layers.

Performance of the actuators are experimentally characterized in quasi-static and dynamic experiments. The quasi-static experiments measure the voltage-deflection curves upon unipolar sinusoidal excitation (1 Hz, 5 s duration), starting with a 10 V amplitude and increasing the voltage in 10 V increments, until breakdown. The dynamic experiments measure frequency responses of the actuators in response to a unipolar sinusoidal stimulation with a 400 V_{pp} amplitude are applied at 300 incrementally increasing frequencies, logarithmically distributed over the 1 Hz to 1 kHz interval.

An experimental set-up is built for the actuation measurements, as shown in Figure 4. Actuator is placed in a clamp that fixes it in place vertically, and provides electrical connections. Voltage is applied from a PC computer running a Labview 2018 environment (National Instruments) via a data acquisition board (National Instruments USB-6211) and a high-voltage amplifier (Smart Materials HVA 1500/50). Actuator deflections are measured using a laser displacement sensor (Micro-Epsilon OptoNCDT 1402-10), digitized (NI USB-6211), and further captured and stored in the same PC running Labview 2018.

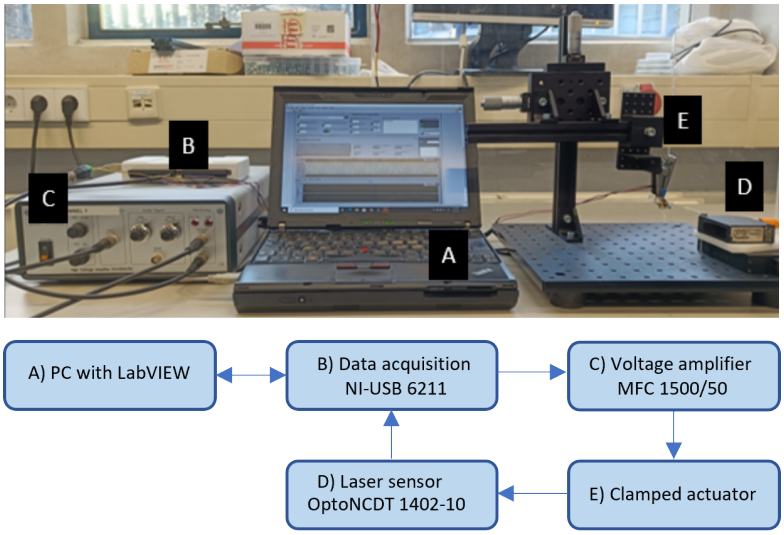

Figure 4. The experimental set-up for measuring actuation performance.

3. RESULTS

3.1 Fabrication

Bottom electrode fabrication (following Section 2.3.1) produced well-conducting Ag layers that measured $< 1\ \Omega$ in resistance from contact pad to the tip of the actuator on the IJ-220 substrate, and between 10 Ω and 100 Ω on the PEN substrate (Voltcraft VC860 multimeter). The resulting electrode is shown in Figure 5a. The P(VDF-TrFE-CTFE) ink was then stencil-printed on the bottom electrode (following Section 2.3.2), producing a uniform EAP layer, as shown in Figure 5b. Next, the top electrode was inkjet-printed on the EAP layer (according to Section 2.3.3), and the printed and cured top electrodes attained a base-to-tip resistances between 2 Ω to 300 Ω. An actuator sample after printing the top electrode is shown in Figure 5c, and a finished sample after separating it from the substrate by laser-cutting is shown in see Figure 5d.

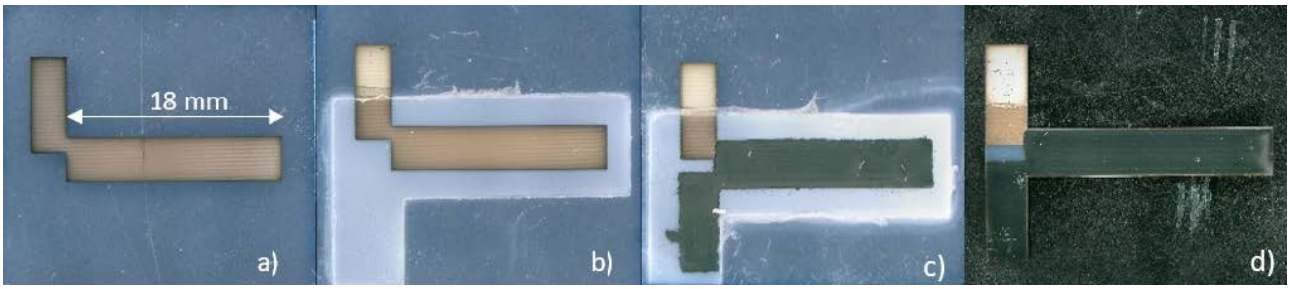

Figure 5. Intermediate results of the actuator fabrication process, showing the actuator sample after: a) inkjet-printing the bottom electrode on a PEN or PET-based substrate; b) stencil-printing the EAP layer; c) inkjet-printing the top electrode; and d) laser-cutting the sample to separate the actuator from the rest of the substrate.

Basing on the proposed process (Section 2.3), actuator samples were fabricated basing on both the PEN and IJ-220 substrates. A series of samples with a different EAP layer thickness were manufactured on the IJ-220 substrate, using total stencil thicknesses of 0.2 mm up to 1 mm. Fabrication on the PEN substrate was more challenging, and therefore these actuator samples only based on the 0.5 mm stencil.

3.2 Actuator structure

Actuator cross-section was studied according to Section 2.4, and the layer thicknesses were measured basing on the SEM images. As can be seen in Figure 6, the (approximately 140 μm thick) substrate (IJ-220) constitutes

the majority of the actuator thickness. The bottom electrode does not show distinct boundaries that can be measured, since it is absorbed into the porous coating. The EAP layer thicknesses measured 3 μm to 24 μm, respectively for the stencil thicknesses of 0.2 mm to 1 mm, and these results are given in Figure 7. The top electrodes measured consistently between 2 μm and 3 μm in thickness.

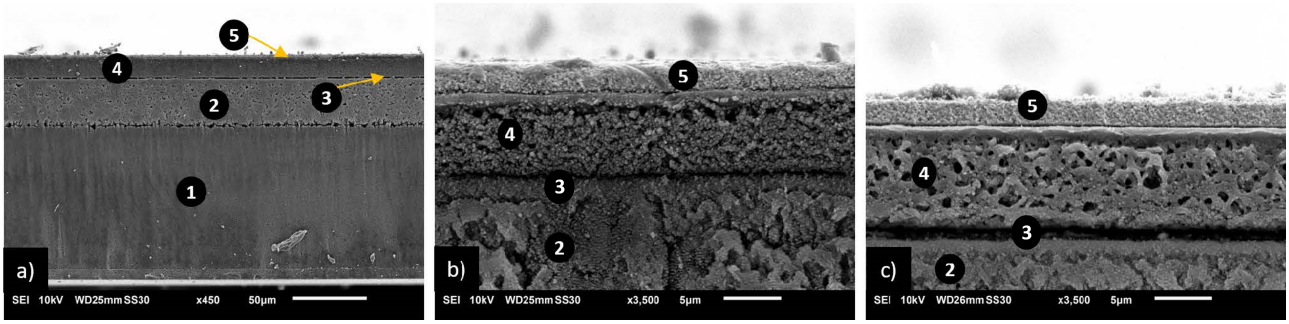

Figure 6. SEM images of the actuator cross-sections: a) the entire thickness of an actuator; b) close-up of a well-performing actuator; and c) close-up of an actuator with a short-circuit between the top and bottom electrodes. Labels indicate the actuator components: 1 – PET portion of the IJ-220 substrate; 2 – microporous resin portion of the IJ-220 substrate; 3 – the bottom electrode; 4 – the P(VDF-TrFE-CTFE) layer (5 - 24 μm); and 5 – the top electrode (2 - 3 μm).

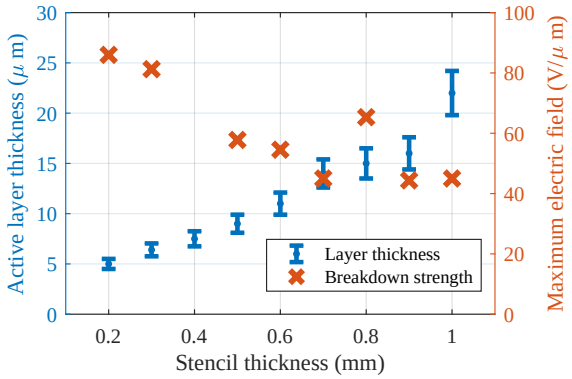

Figure 7. Polymer layer thicknesses (left axis) and breakdown strengths (right axis) versus the respective stencil thickness that was used to fabricate the samples. Breakdown strength is missing for the actuator that corresponds to the 0.4 mm stencil thickness since it was faulty (short-circuit through the EAP layer).

3.3 Actuation performance

Quasi-static tip deflections of the unimorph actuator were modelled according to Section 2.1. The results corresponding to the 50 μm and 140 μm thick substrates in combination with an EAP layer of $0 - 300$ μm thickness are plotted in Figure 8. Printing optimal EAP thicknesses was not realized in this study due to practical limitations. The substrate thicknesses would require optimal EAP thicknesses of 40 μm and above, requiring multiple kV activation voltages (the available amplifier is insufficient) or fabricating it in a stack of multiple EAP layers (laborious and out of the scope of this study). Therefore, fabrication was implemented basing on stencil thicknesses of up to 1 mm.

Actuation in response to quasi-static and dynamic stimulation was measured according to Section 2.4, and an actuator sample during the experiments is shown in Figure 12. The voltage-deflection curves upon a 1 Hz stimulation at incrementally increasing voltages (from 10 V_{pp} until breakdown) are shown in Figure 9 for all actuators. For one of the actuator samples the respective tip deflection profiles are shown in time domain in Figure 10 (showing every tenth applied voltage amplitude). The maximum tolerable electric fields (before

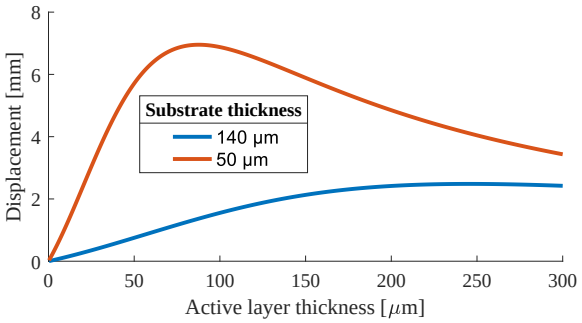

Figure 8. Model prediction of the actuator tip displacement. The two lines correspond to the IJ-220 and PEN substrates, showing the anticipated tip displacement as a function of the EAP layer thickness (assuming EAP strains of 0.5%).

breakdown) were calculated, and are shown alongside the EAP layer thickness measurement results in Figure 7. Frequency response measurements were conducted on the same samples at a 400 V_{pp} stimulation amplitude, and are plotted for three actuator samples in Figure 11. Using lower than maximum voltages served to prevent damaging the samples before the voltage-deflection curves were measured. Besides the quasi-static gain, several resonances and anti-resonance are seen, corresponding to the vibration modes of a cantilever beam.

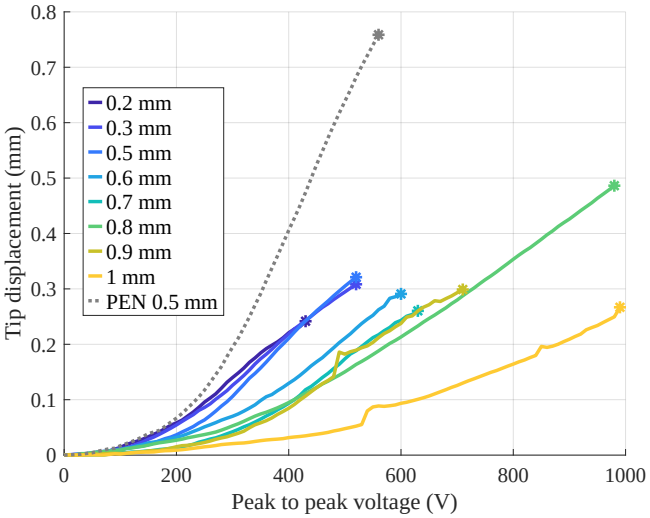

Figure 9. Voltage-displacement curves of the actuator samples in response to unipolar sinusoidal excitation at a 1 Hz frequency and incrementally increasing amplitude. Eight samples base on the IJ-220 substrate and one bases on the PEN substrate. The markers in the end of the traces indicate breakdown.

For IJ-220 substrate, the sample with a 15 μm thick EAP layer (corresponding to the 0.8 mm thick stencil) attained the highest quasi-static strains of up to 486 μm (980 V). Additional measurements showed up to 4.44 mm resonant deflections upon 700 V_{pp} excitation at 116 Hz. The PEN-based samples produced up to 759 μm quasi-static displacements (560 V_{pp}) and up to 3.7 mm resonant deflections (52 Hz, 400 V_{pp}). For comparison, the respective IJ-220 sample of the same stencil thickness (0.5 mm) attained 321 μm quasi-static displacements (520 V_{pp}) and 3.21 mm resonant displacements (119 Hz, 400 V_{pp}). Additional measurements showed resonant deflections of up to 5.95 mm in response to 550 V_{pp} excitation (52 Hz). The resonant frequencies differ significantly between the substrates due to the IJ-220 being much thicker and stiffer. Resonant operation significantly increases the tip deflection over the quasi-static operation, with a Q factor of 11 to 18.

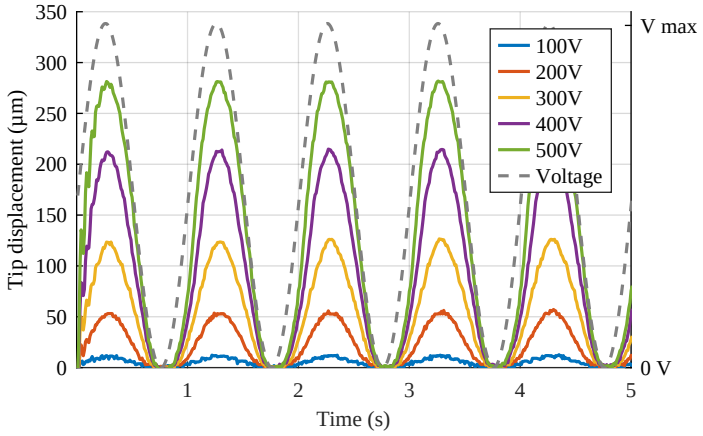

Figure 10. Actuation response of one of the samples during the voltage-deflection measurements (IJ-220 substrate, 6 μm thick EAP, 0.3 mm stencil). The measurements were conducted in 10 V increments, and the figure shows every 10th result, i.e. 100 V increments.

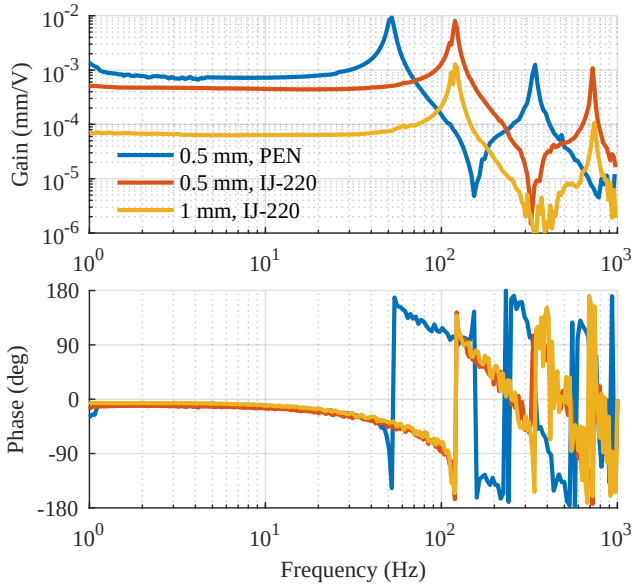

Figure 11. Frequency responses of three actuator samples: (1) PEN substrate in combination with an EAP layer printed using a 0.5 mm stencil; (2) IJ-220 substrate with an EAP layer printed using a 0.5 mm stencil; and (3) IJ-220 substrate with an EAP layer printed using a 1 mm stencil. The responses were measured at a 400 V_{pp} amplitude.

4. DISCUSSION

4.1 Fabrication

4.1.1 Bottom electrode

Printing the bottom electrode was significantly less complex on the IJ-220 substrate than on PEN, allowing to print sharp patterns and line widths of down to approximately 25 μm. The smooth and hydrophilic surface of the PEN substrate had to be first treated to improve its wettability. This was implemented using laser treatment, by etching a dotted pattern into the surface, significantly improving the wettability, but causing spreading of the ink. While this did not impact actuator fabrication, it deteriorated the printing resolution and ability to

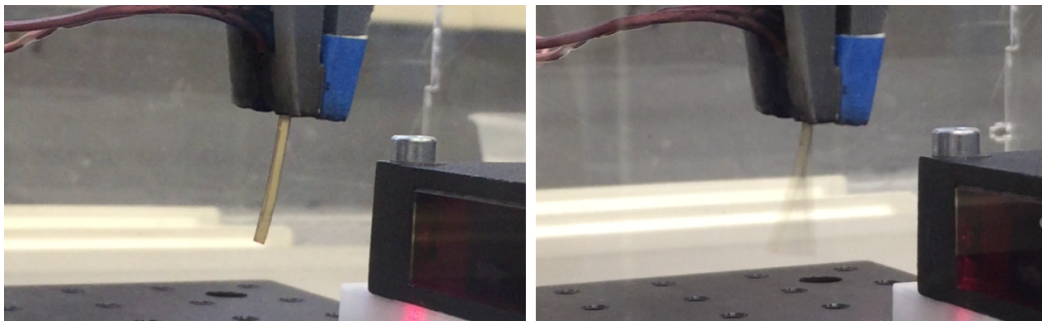

Figure 12. An actuator sample under quasi-static (left) and resonant (right) excitation.

produce small feature sizes. Printing of the electrodes resulted in a strong adhesion on both substrates, showing no Ag separation in scotch tape pull tests.

Achieving a condictive electrode required the printing resolution to be high enough for the adjacent droplets to make contact (or overlap) after deposition. On the porous IJ-220 substrate this was achieved by printing at a 1000 DPI resolution, producing a thin electrode layer that consists of individual overlapping lines. On PET, printing at a 1500 DPI resolution was repeated for four times to deposit enough material to attain a conductive electrode (Samba printhead has a much smaller droplet volume than DMC, Table 1), while the wetting and spreading of the ink facilitated formation of a uniform layer.

Deterioration of the jetting characteristics and occasional clogging of the nozzles was observed during printing. The affected nozzles deviate in droplet volume and jetting direction, causing misplacement and reduction of the deposited material. The clogged nozzles caused missing lines in the electrode layer, rendering it non-conductive. Therefore, the Mitsubishi NBSIJ-MU01 ink (Dimatix DMC printhead) was printed using only one nozzle, attaining consistent results at the cost of the increased printing time. Printing the Metalon JS-A211 (Dimatix Samba printhead) was conducted using all 12 nozzles, requiring regular inspections and purging procedures.

4.1.2 EAP layer

Stencil printing proved as a versatile method for fabricating the EAP layer. Clamping the stencil by magnets made it straight-forward to apply the EAP ink, while the lifting was complicated by the sticking of the polymer to the rough edges of the stencil. On IJ-220, the polymer ink made a strong bond with the porous coating (EAP layer footprint is larger than the bottom electrode), allowing to lift the stencil without causing any damage. On PEN, adhesion of the EAP to the substrate was weaker, and a scalpel had to be used to detach the stencil edges.

The resulting EAP layer thickness showed a linear increase with the stencil thickness (Figure 7, 5 μm to 24 μm for 0.2 mm to 1 mm stencil thicknesses), whereas the observed variations are hypothesized to stem from the printing process being a manual and contact-based method. Stencil printing was made easy due to the simple geometry of the actuators in this study. Printing more complex geometries using a stencil is complicated by the sweeping tool potentially deforming the finer features of the stencil, and implementing uncovered islands is virtually impossible by this method.

4.1.3 Top electrode

The plasma-treated EAP surface behaved during the top electrode printing similarly to the laser-treated PEN substrate during the bottom electrode fabrication. The Ag ink droplets exhibited some spreading on the non-porous and hydrophilic EAP surface, deteriorating the printing resolution and causing the wet ink to flow upon fast printbed motion. The deteriorated resolution made the effects of misaligned and clogged nozzles less critical, allowing to use all 12 nozzles, therefore reducing the total printing time.

The manual steps of plasma treatment and printhead servicing made the top electrode fabrication more laborious than the bottom electrode. Oxygen plasma treatment resulted in a strong adhesion, which was confirmed by scotch tape pulling tests, showing no Ag separation. Four printing iterations at 1500 DPI resolution were required to deposit enough Ag ink to reliably form a conductive electrode after sintering. Regular inspections

and occasional servicing (purging and cleaning) were required to prevent nozzle clogging and the respective line defects that would render the electrode non-conductive (resistance $> 1\ M\Omega$).

4.2 Actuator structure

Imaging the actuator cross-sections in SEM allowed to measure the constituent layer thicknesses and provided insights into their performance and failures. The most common failures in actuator fabrication were poor electrode conductivity ($> 1M\Omega$ from base to tip) and short-circuit between the top and bottom electrodes. Poor conductivity was mainly caused by jetting failures and the respective insufficient material deposition. Short-circuits between the top and bottom electrodes were associated with the observation of porosity in the EAP layer. SEM images showed a dense EAP layer in the functional samples, while the faulty samples were more porous in structure (Figure 6). It is hypothesized that the conductive ink seeps into the porous EAP layer, short-circuiting the electrodes or lowering the dielectric breakdown strength. A dense and homogeneous EAP layer is essential to withstand high field strengths and produce high strains.

While the cause of this inconsistency in polymer structure was not identified, the possible causes are the variations in the manual process of stencil printing (exposure time of the ink to air before swiping and the speed of swiping) and solvent evaporation dynamics in the varying environment conditions (temperature and air humidity). Presence of water residues in the substrate (from air humidity or printing the bottom electrode) can cause porosity due to the non-solvent induced phase separation.

4.3 Actuation response

Characterization of the actuation capabilities showed very large displacements for this type of actuators. The previously reported similar P(VDF-TrFE-CTFE) actuators showed up to 340 μm um of quasi-static displacements and 3.7 mm resonant displacements (at 104 Hz).[21,22,30] Therefore the actuators basing on the PEN and IJ-220 substrates respectively attained 123 % (i.e. 759 μm, 560 V_{pp}) and 42% (i.e. 486 μm, 980 V_{pp}) larger quasi-static displacements. Resonant displacements for the PEN and IJ-220 samples respectively attained a 60% (i.e. 5.95 mm, 550 V_{pp}, 52 Hz) and an 18% (4.44 mm, 700 V_{pp}, 116 Hz) improvement over the prior art. Maximum dielectric breakdown field strenghts of approximately 80 $V/\mu m$ were observed, which is better than the 44 $V/\mu m$ reported for spray-printed actuators,[22] but lower than the 200 $V/\mu m$ reported for solution-casted actuators and the $> 350\ V/\mu m$ dielectric strength specified by the P(VDF-TrFE-CTFE) manufacturer.[11]

Voltage-displacement behaviour of the actuators (Figures 8 and 9) is clearly non-linear at low strains, but follows a roughly proportional trend at larger strains. Therefore, the behaviour at low displacements is consistent with the quadratic strain-field relation of the relaxor ferroelectrics. The increasingly proportional relation at higher strains is most probably caused by the strains exceeding the validity region of the linear beam behaviour. Furthermore, while the thicker EAP layers should have produced larger total tip deflections than the thinner ones (Figure 8), this was not confirmed in experiments (Figure 9). Increasing the EAP layer thickness indeed increased the actuator breakdown voltages (Figure 9), but deteriorated their dielectric breakdown field strengths (Figure 7). This is most probably caused by the EAP layer porosity, and it is anticipated that the model predictions are met (Figure 8) once the challenges in EAP densification are resolved.

The EAP layer had a very small contribution to the actuator stiffness, indicated by a negligible variation in the resonant frequency with the layer thickness (see IJ-220 results in Figure 11). This is explained by the much lower Young's modulus (20x difference in the model) and layer thickness (contributing between 3% and 15% of the total thickness) of P(VDF-TrFE-CTFE) with respect to the substrate. The differences in actuation output between the PET- and PEN-based samples indicates that substrate properties and EAP thickness have significant impact on actuation (Figure 9), as predicted by the model (Figure 8). The PEN substrate is much thinner and softer, as can also be seen in the much lower resonant frequency (Figure 11) and higher tip displacements (Figure 9).

Actuators with a varying EAP layer thicknesses were implemented only on IJ-220, since the fabrication process was less laborious to implement on this substrate, than on PEN. EAP layers were fabricated between 5 μm and 24 μm in thickness, which is well below the ideal (see Figure 8). Thicker EAP layers were not fabricated in this study for practical limitations, i.e. the amplifier cannot supply high enough voltage ($> 1.5\ kV$) to characterize such actuators in a single EAP layer configuration, and challenges in fabricating stacked actuators

(i.e. stacking multiple thinner layers to maintain low operating voltages) were not yet resolved. Therefore, the realized actuators remain in the lower end of the attainable strains, and a significant increase is viable in actuation displacements when thicker EAP layers or thinner substrates are employed (Figure 8). This bases on the assumptions of 0.5% material strains (well below the up to 5% P(VDF-TrE-CTFE) strain specified by the supplier[11]) and ignores the electrode thicknesses (very thin and softer than bulk Ag).

5. CONCLUSIONS

This study proposed a process for fabricating P(VDF-TrFE-CTFE) actuators that combines inkjet printing and stencil printing. Stencil printing was employed for the first time in EAP transducer fabrication and proved an effective method for depositing EAP inks. Actuator fabrication addressed ink adhesion challenges on the smooth PEN surface via laser-etching a dot pattern in it, and on the smooth EAP surface via plasma treatment, while the porous coating on the IJ-220 substrate did not require any treatment. Drying and curing processes were implemented via heating. Further research is required into densification of the polymer layer during drying and curing, and into optimizing the wetting properties of the EAP surface. The effect of dimensions and properties of the actuator constituent materials were analytically modelled and accounted in estimating actuation performance and optimal morphology.

Actuators were manufactured on 140 μm-thick PET-based flexible substrates with the EAP layer thickness of 5 μm to 24 μm, and on 50 μm-thick PEN substrates with EAP layer thickness of 10 μm. The PEN-based actuators achieved tip deflection up to 759 μm in response to 1 Hz sinusoidal excitation at 560 V_{pp}, and up to 5.95 mm under resonant operation at 52 Hz (550 V_{pp}). The PET-based actuators achieved tip deflection up to 486 μm in response to 1 Hz sinusoidal excitation at 980 V_{pp}, and up to 4.44 mm deflection under resonant operation at 116 Hz (700 V_{pp}). This means up to 123% higher quasi-static and up to 60% higher resonant deflections than priorly reported for similar actuators. While optimal EAP layer thicknesses were not printed in this study due to practical limitations, modelling shows that even larger actuation displacements can be attained.

REFERENCES

[1] Soto, F., Karshalev, E., Zhang, F., Esteban Fernandez de Avila, B., Nourhani, A., and Wang, J., "Smart materials for microrobots," *Chemical Reviews* **122**, 5365–5403 (Mar 2022).

[2] Motreuil-Ragot, P., Hunt, A., Kasi, D., Brajon, B., Maagdenberg, A. v. d., Orlova, V., Mastrangeli, M., and Sarro, P. M., "Enabling actuation and sensing in organs-on-chip using electroactive polymers," in [*2020 3rd IEEE International Conference on Soft Robotics (RoboSoft)*], 530–535 (2020).

[3] Sideris, E. A., de Lange, H. C., and Hunt, A., "An ionic polymer metal composite (ipmc)-driven linear peristaltic microfluidic pump," *IEEE Robotics and Automation Letters* **5**(4), 6788–6795 (2020).

[4] Le, M. Q., Capsal, J.-F., Galineau, J., Ganet, F., Yin, X., Yang, M. D., Chateaux, J.-F., Renaud, L., Malhaire, C., Cottinet, P.-J., and Liang, R., "All-organic electrostrictive polymer composites with low driving electrical voltages for micro-fluidic pump applications," *Scientific Reports* **5**, 11814 (Jul 2015).

[5] Bahl, S., Nagar, H., Singh, I., and Sehgal, S., "Smart materials types, properties and applications: A review," *Materials Today: Proceedings* **28**, 1302–1306 (2020). International Conference on Aspects of Materials Science and Engineering.

[6] Stuart, M. A. C., Huck, W. T. S., Genzer, J., Müller, M., Ober, C., Stamm, M., Sukhorukov, G. B., Szleifer, I., Tsukruk, V. V., Urban, M., Winnik, F., Zauscher, S., Luzinov, I., and Minko, S., "Emerging applications of stimuli-responsive polymer materials," *Nature Materials* **9**, 101–113 (Feb 2010).

[7] Sobczyk, M., Wiesenhütter, S., Noennig, J. R., and Wallmersperger, T., "Smart materials in architecture for actuator and sensor applications: A review," *Journal of Intelligent Material Systems and Structures* **33**(3), 379–399 (2022).

[8] Leo, D. J., [*Engineering analysis of smart material systems*], John Wiley & Sons (2007).

[9] Bar-Cohen, Y. and Zhang, Q., "Electroactive polymer actuators and sensors," *MRS Bulletin* **33**, 173–181 (Mar 2008).

[10] Bar-Cohen, Y., "Electroactive polymers as an enabling materials technology," *Proceedings of the Institution of Mechanical Engineers, Part G: Journal of Aerospace Engineering* **221**(4), 553–564 (2007).

[11] "Piezotech RT-TS," (2020). Piezotech Arkema-CRRA: Rue Henri Moissan, 69496 Pierre-Benite Cedex, France.

[12] Bar-Cohen, Y., Cardoso, V., Ribeiro, C., and Lanceros-Méndez, S., "Chapter 8 - electroactive polymers as actuators," in [*Advanced Piezoelectric Materials (Second Edition)*], Uchino, K., ed., *Woodhead Publishing in Materials*, 319–352, Woodhead Publishing, second edition ed. (2017).

[13] Lheritier, P., Noel, S., Vaxelaire, N., Domingues Dos Santos, F., and Defay, E., "Actuation efficiency of polyvinylidene fluoride-based co- and ter-polymers," *Polymer* **156**, 270–275 (2018).

[14] Jo, C., Pugal, D., Oh, I.-K., Kim, K. J., and Asaka, K., "Recent advances in ionic polymer–metal composite actuators and their modeling and applications," *Progress in Polymer Science* **38**(7), 1037–1066 (2013).

[15] Nabawy, M. R. A., Parslew, B., and Crowther, W. J., "Dynamic performance of unimorph piezoelectric bending actuators," *Proceedings of the Institution of Mechanical Engineers, Part I: Journal of Systems and Control Engineering* **229**(2), 118–129 (2015).

[16] Wang, Q.-M. and Cross, L. E., "Performance analysis of piezoelectric cantilever bending actuators," *Ferroelectrics* **215**(1), 187–213 (1998).

[17] Gonçalves, S., Serrado-Nunes, J., Oliveira, J., Pereira, N., Hilliou, L., Costa, C. M., and Lanceros-Méndez, S., "Environmentally friendly printable piezoelectric inks and their application in the development of all-printed touch screens," *ACS Applied Electronic Materials* **1**, 1678–1687 (Aug 2019).

[18] Baelz, K. K. and Hunt, A., "P(vdf-trfe-ctfe) actuators with inkjet printed electrodes," in [*2019 7th International Conference on Control, Mechatronics and Automation (ICCMA)*], 327–332 (2019).

[19] Della Schiava, N., Thetpraphi, K., Le, M.-Q., Lermusiaux, P., Millon, A., Capsal, J.-F., and Cottinet, P.-J., "Enhanced figures of merit for a high-performing actuator in electrostrictive materials," *Polymers* **10**(3) (2018).

[20] Oh, S. R., Wong, T. C., Tan, C. Y., Yao, K., and Tay, F. E.-H., "Fabrication of piezoelectric polymer multilayers on flexible substrates for energy harvesting," *Smart Materials and Structures* **23**, 015013 (dec 2013).

[21] Sekar, S. A. and Hunt, A., "Inkjet printing p(vdf-trfe-ctfe) actuators for large bending strains," *Smart Materials and Structures* **33**, 025036 (jan 2024).

[22] IJssel de Schepper, S. and Hunt, A., "An airbrush 3d printer: Additive manufacturing of relaxor ferroelectric actuators," *Additive Manufacturing* **81**, 103982 (2024).

[23] Pan, J., Tonkay, G., Storer, R., Sallade, R., and Leandri, D., "Critical variables of solder paste stencil printing for micro-bga and fine-pitch qfp," *IEEE Transactions on Electronics Packaging Manufacturing* **27**(2), 125–132 (2004).

[24] Otte, S., "Polymer stencil printing for high-throughput fabrication of metamaterials," (2022).

[25] Della Schiava, N., Pedroli, F., Thetpraphi, K., Flocchini, A., Le, M.-Q., Lermusiaux, P., Capsal, J.-F., and Cottinet, P.-J., "Effect of beta-based sterilization on p(vdf-trfe-cfe) terpolymer for medical applications," *Scientific Reports* **10**, 8805 (May 2020).

[26] "Novele ij-220 printed electronics substrate - inkjet receptive," (2011). NCC Nano LLC dba NovaCentrix: 400 Parker Drive, Suite 1110, Austin, TX 78728.

[27] ChemTel Inc., "NBSIJ-MU01 (Silver Nano Particle Ink) Safety Data Sheet," (2019).

[28] Novacentrix, "Metalon JS-A211 Nanosilver Ink – Aqueous dispersion for Inkjet Printing," (2020).

[29] Obilor, A. F., Pacella, M., Wilson, A., and Silberschmidt, V. V., "Micro-texturing of polymer surfaces using lasers: a review," *The International Journal of Advanced Manufacturing Technology* **120**, 103–135 (May 2022).

[30] Baelz, K. and Hunt, A., "P(vdf-trfe-ctfe) actuators with inkjet printed electrodes," in [*7th International Conference on Control, Mechatronics and Automation (ICCMA)*], 327–332 (11 2019).